RECOVERING A FUNCTION FROM ITS INTEGRALS OVER CONICAL SURFACES THROUGH RELATIONS WITH THE RADON TRANSFORM

FATMA TERZIOGLU

Abstract. This paper addresses the overdetermined problem of inverting the n-dimensional cone (or Compton) transform that integrates a function over conical surfaces in $\mathbb{R}^n$. The study of the cone transform originates from Compton camera imaging, a nuclear imaging method for the passive detection of gamma-ray sources. We present a new identity relating the n-dimensional cone and Radon transforms through spherical convolutions with arbitrary weight functions. This relationship, which generalizes a previously obtained identity, leads to various inversion formulas in n-dimensions under a mild assumption on the geometry of detectors. We present two such formulas along with the results of their numerical implementation using synthetic phantoms. Compared to our previously discovered inversion techniques, the new formulas are more stable and simpler to implement numerically.

1. Introduction

We address analytic inversion of the *cone transform* that is defined for a function f on $\mathbb{R}^n$ by

$$Cf(u,\beta,\psi) = \int_{\mathfrak{S}_{u,\beta,\psi}} f(x)dS(x), \tag{1}$$

where $dS(x)$ denote the Lebesgue measure on the surface cone

$$\mathfrak{S}_{u,\beta,\psi} = \{x \in \mathbb{R}^n : (x-u)\cdot\beta = |x-u|\cos\psi\}.$$

Here, $u \in D \subset \mathbb{R}^n$ denotes the vertex (apex) of a cone and D is the set of cone vertices (which can be lower dimensional than n), $\beta \in \mathbb{S}^{n-1}$ is cone's central axis direction and $\psi \in (0,\pi)$ is the (half-)opening angle (see fig. 1(b)). We denote the unit sphere in $\mathbb{R}^n$ by $\mathbb{S}^{n-1}$, and its area by $|\mathbb{S}^{n-1}|$ (we consider $|\mathbb{S}^0| = 2$).

In the case that the support of the integrand f is required to be disjoint from the set of cone vertices D, the integral (1) is also called *the Compton transform*. This terminology is due to that the data provided by a γ-ray detection system called *Compton camera* (fig. 1(b)) can be modeled

2020 *Mathematics Subject Classification.* Primary 65R32; Secondary 92C55.

Key words and phrases. cone transform, inversion, exact, Compton camera, reconstruction.

as (weighted) integrals of the radiation source distribution over conical surfaces having vertex on the scattering detector. Hence, one can obtain the source distribution map by inverting the Compton transform. More information about Compton camera imaging can be found, for example, in [1–8] and references there.

In the integral model of the realistic Compton camera measurements, one may need to include some non-unit integration weights [4, 9]. Variations of (1) corresponding to different integration weights, some of which originated from the Compton imaging application, were considered in [4, 7, 10–13, and references therein]. Some analytic properties of the cone transform were studied in [12, 14, 15].

Cone transform inversion is an overdetermined problem because the dimension of the space of cones in $\mathbb{R}^n$ is equal to $n+\dim(D)$, which is greater than n unless D is a singleton. Therefore, it is expected that there would be multiple left inversions that agree on the ideal measurements but behave differently in the case of noisy measurements. Several inversion formulas for the cone transform with pure surface measure on the cone exist in the literature ([1–3, 7, 16–27, see also their references]). In some of the references listed above, an $n-$dimensional subset of the space of cones was chosen and hence a unique inversion formula was derived. In this paper, we consider all possible cones with vertices in a given set D, and eliminate the extra parameters by averaging over them later in the reconstruction process. This has the advantage of reducing the noise present in the forward data and hence stabilizing the reconstruction. We also note that the developed formulas are independent of the geometry of the vertex set D as long as it satisfies a nonrestrictive assumption.

To the author's knowledge, inverting the cone transform by exploiting its relation with the Radon transform was first proposed in [3]. Later, in [7], the three-dimensional cone and the Radon transforms were linked via an integral identity involving integration of the cone transform with respect to the opening angles and convolution of the Radon transform with respect to the affine variable. A generalization of this integral relation for weighted cone transforms in n-dimensions was presented in [11]. In a previous work, we formulated yet another relation between the cone and the Radon transforms: the sine-weighted average of the cone transform of a function with respect to opening angles is a special spherical convolution (called the cosine transform) of the Radon transform of that function (see [20, Theorem 5]). This led to a new reconstruction procedure based on the inversion of the cosine transform [20, 21]. Although we were able to successfully reconstruct the images, doing so was difficult due to the differentiations that the algorithm required. In this paper, we generalize this relation in such a way that it admits arbitrary spherical convolution kernels. The flexibility in the choice of the convolution kernel leads to a wider variety of inversion methods, some of which, as we show, are more stable and simpler than the previous formula obtained in [20, 21].

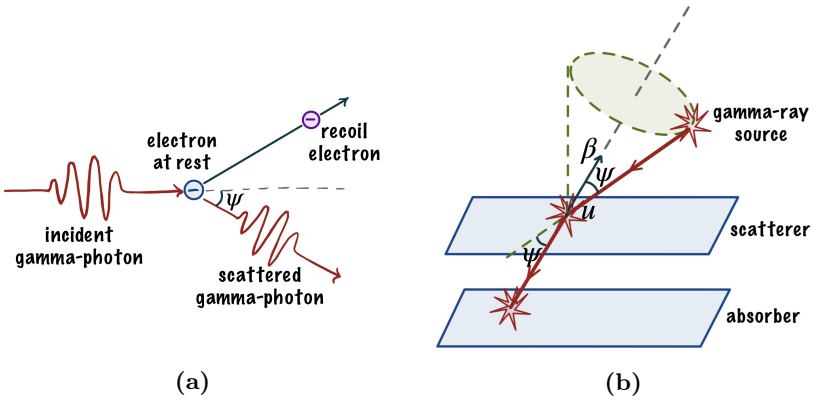

Figure 1. *Schematic representation of* **(a)** *Compton scattering principle and* **(b)** *a planar Compton camera consisting of double layer position and energy sensitive detectors. When an incoming gamma photon hits the camera, it undergoes Compton scattering in the front detector (scatterer) and photoelectric absorption in the second detector (absorber). The recorded energies and the positions of interactions on both detectors provide a cone of possible incident directions of the gamma-ray.*

The paper is organized as follows. In section 2, we recall some relevant integral transforms and their properties. Section 3 includes the formulation of the integral identity relating n-dimensional cone and Radon transforms via spherical convolutions (theorem 3.1). In section 4, we outline how this relation can be used in deriving a family of inversion formulas for the n-dimensional cone transform. Then, we present two inversion formulas (theorems 4.1 and 4.4) and discuss the condition on the set of cone vertices that guarantee stable reconstruction. Section 5 contains the results of the numerical implementation of the proposed inversion formulas in dimension three.

2. Preliminaries

We first recall that the n-dimensional Radon transform of a function f on $\mathbb{R}^n$ is defined by the integral

$$Rf(\omega, s) = R_s f(\omega) = \int_{x\cdot\omega=s} f(x)dx, \tag{2}$$

where $x \cdot \omega = s$ is the equation of the hyperplane orthogonal to $\omega \in \mathbb{S}^{n-1}$ at the signed distance $s \in \mathbb{R}$ from the origin. The following well known inversion formula for the Radon transform will be useful in the sequel (see

e.g. [28–30]). For any smooth fast decaying function $f \in \mathcal{S}(\mathbb{R}^n)$,

(3)
$$f(x) = \frac{(2\pi)^{1-n}}{2} \begin{cases} (-1)^{(n-1)/2} \int\limits_{\mathbb{S}^{n-1}} (Rf)^{(n-1)}(\omega, x\cdot\omega)d\omega, & \text{if } n \text{ is odd,} \\ (-1)^{(n-2)/2} \int\limits_{\mathbb{S}^{n-1}} \mathcal{H}(Rf)^{(n-1)}(\omega, x\cdot\omega)d\omega, & \text{if } n \text{ is even,} \end{cases}$$

where $\mathcal{H}$ is the Hilbert transform in $\mathbb{R}$ defined as the principal value integral

$$\mathcal{H}g(t) = \frac{1}{\pi} p.v. \int\limits_{\mathbb{R}} \frac{g(s)}{t-s} ds,$$

and

$$(Rf)^{(n-1)}(\omega, s) := \frac{\partial^{n-1}}{\partial s^{n-1}} R(\omega, s).$$

The Funk transform of a continuous function g on $\mathbb{S}^{n-1}$ is defined, for any $\sigma \in \mathbb{S}^{n-1}$, by

$$Fg(\sigma) = \int\limits_{\mathbb{S}^{n-1}\cap\sigma^{\perp}} g(\omega) d_\sigma\omega = \int\limits_{\mathbb{S}^{n-1}} g(\omega)\delta(\omega\cdot\sigma)d\omega, \tag{4}$$

where $d_\sigma\omega$ is the Lebesgue measure on the $(n-2)$-dimensional sphere $\mathbb{S}^{n-1}\cap\sigma^{\perp}$ and δ is the one-dimensional Dirac-delta distribution. Here, the symbol $\sigma^{\perp}$ represents the hyperplane orthogonal to $\sigma \in \mathbb{S}^{n-1}$, and $\omega\cdot\sigma$ denotes the dot product of $\omega, \sigma \in \mathbb{S}^{n-1}$.

It is known that the Funk transform is invertible for smooth even functions on the unit sphere [28,29,31,32]. The following inversion formula for the Funk transform [32, Chapter 5, Theorem 5.37] will be used in the sequel.

Theorem 2.1 ([32], Theorem 5.37)**.** *Let $\varphi = Ff$, $f \in C^{\infty}_{even}(\mathbb{S}^{n-1})$, $n \geqslant 3$. If n is even, then*

$$f = cP(\Delta_S)F\varphi, \quad c = \frac{|\mathbb{S}^{n-1}||\mathbb{S}^{n-2}|}{4\pi^{n-2}},$$

where

$$P(\Delta_S) = 4^{1-n/2} \prod_{k=0}^{(n-4)/2} \left[-\Delta_S + (2k+1)(n-3-2k)\right].$$

If n is odd, then

$$f(\omega) = \int\limits_{\mathbb{S}^{n-1}} \varphi(\beta)d\beta - \frac{2^{n-1}Q(\Delta_S)}{(n-2)!} \int\limits_{\mathbb{S}^{n-1}} \varphi(\beta)\log(|\omega\cdot\beta|)d\beta,$$

where

$$Q(\Delta_S) = 4^{(1-n)/2} \prod_{k=0}^{(n-3)/2} \left[-\Delta_S + (2k+1)(n-3-2k)\right].$$

3. A relation between the cone and the Radon transforms in n-dimensions

In the following, we consider $f \in \mathcal{S}(\mathbb{R}^n)$. However, as in the case of the Radon transform (see, e.g. [30, 33]), the formulas hold in more general function spaces, which can be shown by using extension by continuity (see also section 5 for successful numerical implementations for piecewise continuous phantoms).

We first note that, using the $\delta-$function of a cone's surface, the integral in (1) can explicitly be written as

$$Cf(u,\beta,\psi) = \sin\psi \int_{\mathbb{R}^n} f(x)\delta((x-u)\cdot\beta - |x-u|\cos\psi)dx, \tag{5}$$

where $u \in D \subset \mathbb{R}^n$, $\beta \in \mathbb{S}^{n-1}$, and $\psi \in (0,\pi)$.

Let R and F represent the Radon and the Funk transforms defined in (2) and (4), respectively.

Suppose that h is an integrable function on $[-1,1]$, i.e., $h \in L^1[-1,1]$. For a given $\beta \in \mathbb{S}^{n-1}$, we define $h_\beta(\sigma) := h(\sigma\cdot\beta)$ on $\mathbb{S}^{n-1}$ and let $w_\beta := Fh_\beta$. Then, it is known that

$$Fh_\beta(\sigma) = w_\beta(\sigma) = w(\sigma\cdot\beta), \tag{6}$$

where

$$w(s) = \begin{cases} h\left(\sqrt{1-s^2}\right) + h\left(-\sqrt{1-s^2}\right), & n=2, \\ |\mathbb{S}^{n-3}| \int_{-1}^{1} h(\sqrt{1-s^2}\,t)(1-t^2)^{\frac{n-4}{2}}dt, & n \geqslant 3. \end{cases} \tag{7}$$

For completeness, we present a proof of this fact in the Appendix.

Theorem 3.1. *For any $f \in \mathcal{S}(\mathbb{R}^n)$, $u \in D \subset \mathbb{R}^n$ and $\beta \in \mathbb{S}^{n-1}$,*

$$\int_0^\pi Cf(u,\beta,\psi)w(\cos\psi)d\psi = \int_{\mathbb{S}^{n-1}} Rf(\omega, u\cdot\omega)h(\omega\cdot\beta)d\omega, \tag{8}$$

where the weight functions w and h are related as in (7).

Proof. Let $f \in \mathcal{S}(\mathbb{R}^n)$ and $h(\omega \cdot \beta) = h_\beta(\omega) \in L^1(\mathbb{S}^{n-1})$ for a given $\beta \in \mathbb{S}^{n-1}$. For $u \in D \subset \mathbb{R}^n$, by definition of the Radon transform, we have

$$\begin{aligned}\int\limits_{\mathbb{S}^{n-1}} Rf(\omega, u\cdot\omega)h(\omega\cdot\beta)d\omega &= \int\limits_{\mathbb{S}^{n-1}}\int\limits_{\mathbb{R}^n} f(x)\delta((x-u)\cdot\omega)dx\; h(\omega\cdot\beta)d\omega \\ &= \int\limits_{\mathbb{R}^n} f(x) \int\limits_{\mathbb{S}^{n-1}} \delta((x-u)\cdot\omega)h(\omega\cdot\beta)d\omega\; dx \\ &= \int\limits_{\mathbb{R}^n} f(u+y) \int\limits_{\mathbb{S}^{n-1}} \delta(\frac{y}{|y|}\cdot\omega)h(\omega\cdot\beta)d\omega\; \frac{dy}{|y|},\end{aligned}$$

where we first changed the order of integration, and then changed variables by letting $y = x - u$ and used the homogeneity of δ-distribution. Now since $w_\beta(\omega) = Fh_\beta(\omega)$, in view of (6), we have

$$w(\frac{y}{|y|}\cdot\beta) = \int\limits_{\mathbb{S}^{n-1}} \delta(\frac{y}{|y|}\cdot\omega)h(\omega\cdot\beta)d\omega.$$

Making the substitution

$$\begin{aligned}\frac{1}{|y|}w(\frac{y}{|y|}\cdot\beta) &= \int\limits_{-1}^{1} \frac{1}{|y|}\delta(\frac{y}{|y|}\cdot\beta - t)w(t)dt \\ &= \int\limits_0^\pi \delta(y\cdot\beta - |y|\cos\psi)w(\cos\psi)\sin\psi d\psi,\end{aligned}$$

we finally obtain

$$\begin{aligned}&\int\limits_{\mathbb{S}^{n-1}} Rf(\omega, u\cdot\omega)h(\omega\cdot\beta)d\omega \\ &= \int\limits_{\mathbb{R}^n} f(u+y)\int\limits_0^\pi \delta(y\cdot\beta - |y|\cos\psi)w(\cos\psi)\sin\psi d\psi dy \\ &= \int\limits_0^\pi \sin\psi \int\limits_{\mathbb{R}^n} f(u+y)\delta(y\cdot\beta - |y|\cos\psi)dy\; w(\cos\psi)d\psi \\ &= \int\limits_0^\pi Cf(u,\beta,\psi)w(\cos\psi)d\psi.\end{aligned}$$

□

A special case of this relation, namely for $h(t) = |t|$, was proven in [20] and was used in deriving an inversion formula for the cone transform [20,21]. The advantage of the generalized relationship is that different choices of the convolution kernel lead to various methods for the recovery of the Radon

data, some of which are more stable and/or easier to implement numerically (see the discussion after corollary 4.2).

4. Inversion formulas for the n-dimensional cone transform

In this section, we discuss how the integral relation (8) can be used for recovering the Radon transform of a function from its cone transform data in various ways, and then present two different inversion methods for the n-dimensional cone transform.

4.1. **A method of recovering the Radon transform from the cone transform data.** For a given $\beta \in \mathbb{S}^{n-1}$, let δ_β denote the Dirac-delta distribution on $\mathbb{S}^{n-1}$, and $\mathcal{D}$ be a differential operator on $\mathbb{S}^{n-1}$ admitting a Green's function G_β. Then by letting $h_\beta = G_\beta$, and applying $\mathcal{D}$ in (8) one can formally recover the Radon transform of f. In the following, we derive an inversion formula that is obtained by taking $\mathcal{D}$ as the Laplace-Beltrami operator on $\mathbb{S}^{n-1}$.

Let $n \geqslant 3$, Δ_S denote the Laplace-Beltrami operator on $\mathbb{S}^{n-1}$, and $G_\beta(\sigma)$ be its Green's function for a given $\beta \in \mathbb{S}^{n-1}$, i.e.,

$$\Delta_S G_\beta(\sigma) = \delta_\beta(\sigma) - \frac{1}{|\mathbb{S}^{n-1}|}.$$

It is known that $G_\beta(\sigma) = g_n(\sigma \cdot \beta)$ with

$$g_n(t) = \frac{3-n}{|\mathbb{S}^{n-1}|(n-2)n-1} \frac{1+t}{1-t}\, {}_3F_2\left[\begin{matrix} 1, 1, \frac{5-n}{2} \\ 2, \frac{n+1}{2} \end{matrix}; -\frac{1+t}{1-t}\right] + \frac{1}{|\mathbb{S}^{n-1}|(n-2)} \log\left(\frac{1-t}{2}\right), \tag{9}$$

when n is odd, and

$$g_n(t) = \frac{1}{|\mathbb{S}^{n-1}|(2-n)} \times \sum_{k=0}^{(n-4)/2} \binom{k-\frac{1}{2}}{k} \left[(1-t^2)^{-k} \Big(1 + \frac{t \arccos(-t)}{\sqrt{1-t^2}}\Big) - \frac{1}{3} \sum_{l=1}^{k} \frac{(1-t^2)^{\frac{l-k}{2}}}{\binom{l+\frac{1}{2}}{l-1}} \right], \tag{10}$$

when n is even. Here, ${}_3F_2$ denotes the generalized hypergeometric function defined by

$${}_pF_q\left[\begin{matrix} a_1, \dots, a_p \\ b_1, \dots, b_q \end{matrix}; z\right] = \sum_{k=0}^{\infty} \frac{(a_1)_k \cdots (a_p)_k}{(b_1)_k \cdots (b_q)_k} \frac{z^k}{k!}, \ (a)_k = a(a+1)\dots(a+k-1),$$

(see [34, Theorems 4.3 and 4.7]. We note that the sign difference is due to our consideration of Laplace-Beltrami operator as Δ_S, instead of $-\Delta_S$.)

Now by letting the spherical convolution kernel h in (8) be the function g_n defined above, we obtain the following result.

Theorem 4.1. *Let $n \geqslant 3$ and $f \in \mathcal{S}(\mathbb{R}^n)$. Then, for any $u \in D \subset \mathbb{R}^n$ and $\beta \in \mathbb{S}^{n-1}$,*

(11)

$$Rf(\beta, u\cdot\beta) = \Delta_S \int_0^\pi Cf(u,\beta,\psi) w(\cos\psi) d\psi + \frac{|\mathbb{S}^{n-2}|}{|\mathbb{S}^{n-1}|} \int_0^\pi Cf(u,\beta,\psi) d\psi,$$

where Δ_S acts with respect to the variable β, and

$$w(\sigma\cdot\beta) = w_\beta(\sigma) = FG_\beta(\sigma),$$

which is the Funk transform of G_β, the Green's function of Δ_S.

Proof. Let $G_\beta(\sigma)$ be the Green's function of Δ_S, so $G_\beta(\sigma) = g_n(\sigma\cdot\beta)$ where g_n is as either in (9) or (10), depending the parity of the dimension n.

Applying Δ_S in identity (8) with $h = g_n$ and the corresponding w as given in (7), we obtain

$$\begin{aligned}\Delta_S \int_0^\pi Cf(u,\beta,\psi) w(\cos\psi) d\psi &= \Delta_S \int_{\mathbb{S}^{n-1}} Rf(\omega, u\cdot\omega) G_\beta(\omega) d\omega \\ &= Rf(\beta, u\cdot\beta) - \frac{1}{|\mathbb{S}^{n-1}|} \int_{\mathbb{S}^{n-1}} Rf(\omega, u\cdot\omega) d\omega. \end{aligned} \tag{12}$$

For the integral on the right, we can use (8) with $h(t) = 1$. The Funk transform of the unit function on $\mathbb{S}^{n-1}$ is $|\mathbb{S}^{n-2}|$, so we have $w(s) = |\mathbb{S}^{n-2}|$. Thus,

$$|\mathbb{S}^{n-2}| \int_0^\pi Cf(u,\beta,\psi) d\psi = \int_{\mathbb{S}^{n-1}} Rf(\omega, u\cdot\omega) d\omega. \tag{13}$$

Together with (12), this proves (11). □

Corollary 4.2. *Let $f \in \mathcal{S}(\mathbb{R}^3)$. For any $u \in D \subset \mathbb{R}^3$ and $\beta \in \mathbb{S}^2$,*

(14)

$$Rf(\beta, u\cdot\beta) = \frac{\Delta_S}{2} \int_0^\pi Cf(u,\beta,\psi) \log\left(|\cos\psi| + 1\right) d\psi + \frac{1}{2} \int_0^\pi Cf(u,\beta,\psi) d\psi.$$

Proof. In dimension three ($n = 3$), we have $G_\beta(\sigma) = g_3(\sigma\cdot\beta)$ where $g_3(t) = \dfrac{1}{4\pi} \log\left(\dfrac{1-t}{2}\right)$ by equation (9). Therefore, in view of (6) and (7), we obtain $FG_\beta(\sigma) = w(\sigma\cdot\beta)$ with

$$w(s) = 2\int_0^\pi g_3(\sqrt{1-s^2}\cos\theta) d\theta = \frac{1}{2}\log(1+|s|) - \log 2,$$

(see [35, p. 531, eq. 4.225-12]).

Using theorem 4.1, we obtain

$$Rf(\beta, u\cdot\beta) = \frac{1}{2}\int_0^\pi Cf(u,\beta,\psi)d\psi + \frac{\Delta_S}{2}\int_0^\pi Cf(u,\beta,\psi)\log\left(|\cos\psi|+1\right)d\psi$$
$$-(\log 2)\Delta_S\int_0^\pi Cf(u,\beta,\psi)d\psi.$$

It remains to show that the last term on the right equals zero. Indeed, the Laplace-Beltrami operator Δ_S acts in variable β, and, from the relation (13), we know that $\int_0^\pi Cf(u,\beta,\psi)d\psi$ is independent of β.

□

We remark that our previously obtained inversion formula in [20] involved the application of the Laplace–Beltrami operator twice, while the formula (14) requires its application only once. Since differentiation is an unstable operation numerically, it is expected that (14) leads to more stable reconstructions. This is confirmed by our numerical tests in section 5.

We should also mention that the spherical convolution with kernel $h(t) = \log(1-t^2)$ is known as the zero-order sine transform (see [32, p. 531, eq. (A.13.41)]), and when $n = 3$, it can be inverted by applying the Laplace-Beltrami operator. This also yields (14), which was proven in [36].

Remark 4.3. For $n = 2$, in order to have a nontrivial relation between the cone and the Radon transforms, in view of (6) and (8), the kernel h needs to be the Green's function of a differential operator with order at least two.

In fact, if $h(t) = |t|$, using (7), we have

$$2\int_0^\pi Cf(u,\beta,\psi)\sin\psi d\psi = \int_{\mathbb{S}^1} Rf(\omega, u\cdot\omega)|\omega\cdot\beta|d\omega, \tag{15}$$

Applying $\Delta_S + 1$ in (15) and using the identity

$$(\Delta_S+1)|\omega\cdot\beta| = \delta(\omega\cdot\beta)(1-(\omega\cdot\beta)^2),$$

one obtains

$$2(\Delta_S+1)\int_0^\pi Cf(u,\beta,\psi)\sin\psi d\psi = \int_{\mathbb{S}^1} Rf(\omega,u\cdot\omega)\delta(\omega\cdot\beta)(1-(\omega\cdot\beta)^2)d\omega$$
$$= Rf(\beta^\perp, u\cdot\beta^\perp)(1-(\beta^\perp\cdot\beta)^2) + Rf(-\beta^\perp, -u\cdot\beta^\perp)(1-(-\beta^\perp\cdot\beta)^2)$$
$$= 2Rf(\beta^\perp, u\cdot\beta^\perp),$$

by the evenness of the Radon transform. Hence,

$$Rf(\beta,u\cdot\beta) = (\Delta_S+1)\int_0^\pi Cf(u,\beta^\perp,\psi)\sin\psi d\psi,$$

with Δ_S acting with respect to the variable β. We note that a generalization of this formula to arbitrary even dimensions was proven in [20].

4.2. **An alternative inversion formula.** For $n \geqslant 3$, an alternative formula for recovering Radon projections from cone transform data can be obtained by taking $h(t) = \delta(t)$. Then, in view of (6) and (7), we have $w(\cos\psi) = |\mathbb{S}^{n-3}| \csc\psi$.

Now let T_u denote the operator that shifts a function by $u \in \mathbb{R}^n$. The shift invariance property of the Radon transform implies that $R(\omega, u\cdot\omega) = R(T_u f)(\omega, 0) = R_0(T_u f)(\omega)$, which is a continuous even function on $\mathbb{S}^{n-1}$. Therefore, the relation (8) reduces to

(16)
$$|\mathbb{S}^{n-3}| \int_0^\pi Cf(u,\beta,\psi)\csc\psi d\psi = \int_{\mathbb{S}^{n-1}} Rf(\omega, u\cdot\omega)\delta(\omega\cdot\beta)d\omega = F(R_0(T_u f))(\beta).$$

Now applying the inversion formula for the Funk transform, theorem 2.1, one obtains the following result.

Theorem 4.4. *Let $f \in \mathcal{S}(\mathbb{R}^n)$, $n \geqslant 3$. For $u \in D \subset \mathbb{R}^n$ and $\omega \in \mathbb{S}^{n-1}$, we define*

$$\Phi(u,\beta) := \frac{|\mathbb{S}^{n-3}|}{|\mathbb{S}^{n-1}||\mathbb{S}^{n-2}|} \int_0^\pi Cf(u,\beta,\psi)\csc\psi d\psi.$$

Then, if n is odd,

(17)
$$Rf(\omega, u\cdot\omega) = \int_{\mathbb{S}^{n-1}} \Phi(u,\beta)d\beta - \frac{2^{n-1}Q(\Delta_S)}{(n-2)!} \int_{\mathbb{S}^{n-1}} \Phi(u,\beta)\log(|\omega\cdot\beta|)d\beta$$

where the differential polynomial

$$Q(\Delta_S) = 4^{(1-n)/2} \prod_{k=0}^{(n-3)/2} \left[-\Delta_S + (2k+1)(n-3-2k)\right],$$

acts with respect to the variable ω.

If n is even,

$$Rf(\omega, u\cdot\omega) = \frac{|\mathbb{S}^{n-1}||\mathbb{S}^{n-2}|}{4\pi^{n-2}} P(\Delta_S)(F\Phi)(u,\omega), \tag{18}$$

where $P(\Delta_S) = 4^{1-n/2} \prod_{k=0}^{(n-4)/2} \left[-\Delta_S + (2k+1)(n-3-2k)\right]$ and the Funk transform F act with respect to the variables ω and β, respectively.

Proof. In view of the identity (16), the result follows from applying theorem 2.1 to $\Phi(u,\beta)$ for each fixed $u \in D \subset \mathbb{R}^n$. □

In dimension three, the equation (17) reduces to the following formula.

Corollary 4.5. *Let $f \in \mathcal{S}(\mathbb{R}^3)$. For any $u \in D \subset \mathbb{R}^3$ and $\omega \in \mathbb{S}^2$,*

$$Rf(\omega, u\cdot\omega) = \frac{1}{4\pi^2}\int_{\mathbb{S}^2}\int_0^\pi Cf(u,\beta,\psi)\csc\psi d\psi d\beta + \frac{\Delta_S}{4\pi^2}\int_{\mathbb{S}^2}\int_0^\pi Cf(u,\beta,\psi)\csc\psi d\psi \log|\omega\cdot\beta| d\beta, \tag{19}$$

where Δ_S acts with respect to the variable ω.

After recovering the Radon transform of a function f from its cone transform data using either theorems 4.1 or 4.4, it remains to invert the Radon transform using (3) to obtain the function f. Now if one has access to the complete set of Radon projections, that is $Rf(\beta, s)$ is available for all $s \in \mathbb{R}$ at each direction $\beta \in \mathbb{S}^{n-1}$, then the application of any Radon transform inversion yields the reconstruction of f from its cone transform data. In fact, if any plane intersecting the domain of reconstruction meets a cone vertex, then for all $s \in \mathbb{R}$, we have a $u \in D$ such that $s = u \cdot \beta$. Thus, this condition, which is called the *Compton admissibility condition* [21], guarantees the availability of a complete set of Radon projections. We refer the reader to [21, 36] for a more detailed discussion of admissibility. We note that the same condition was needed in the inversion formulas developed by Smith [7] and was called as *the completeness condition*.

5. Numerical reconstructions

We now present the numerical implementation results of inversion formulas (14) and (19) obtained using `MATLAB`. In the examples below, the phantom was $f = \chi_{B_1} - 0.5\chi_{B_2}$, where $\chi_{B_i}, i = 1, 2$, denotes the characteristic function of the three-dimensional ball with radius 0.3 units and center at the origin, and with radius 0.4 units and center at $(0, 0, -0.4)$, respectively (see fig. 2). The cone projections were simulated by numerically integrating f over a set of discretized cones.

The detector configuration shown in fig. 2(a) was used in the experiments. It was obtained by uniformly sampling a total of 360 points over the two perpendicular great semi-circles (corresponding to points with azimuthal and polar angles of $(\theta_k, \pi/2)$, and $(3\pi/2, \theta_k)$, $\theta_k = k\pi/180$ rad, $k = 1, \ldots, 180$) of the sphere of radius $\sqrt{2}$ units and centered at the origin. An example scanning procedure may involve two small Compton cameras, each moving along a semi-circle, where the points on these semi-circles correspond to the center position of the detector. We remark that before applying the Radon transform inversion after recovering the Radon data of the phantom via theorems 4.1 or 4.4, one needs to apply interpolation or approximation to obtain the Radon data for uniformly sampled affine variables for each given

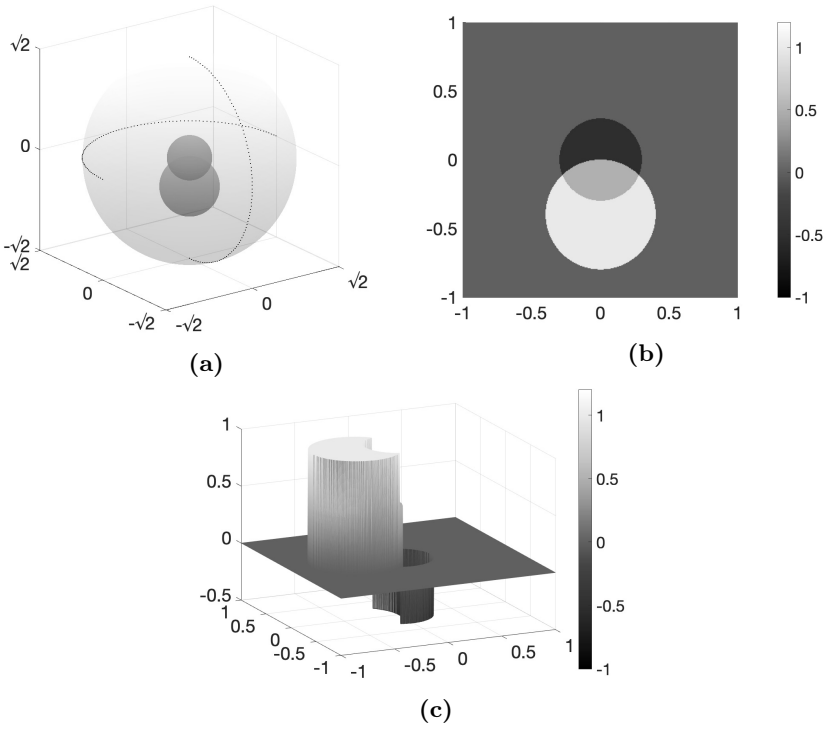

Figure 2. **(a)** *Scanning geometry showing the position of the phantom f in reference to the detector geometry. Black dots represent the detection sites.* **(b)** *The cross-section of the phantom by the plane $x = 0$.* **(c)** *Surface plot of the phantom's cross-section by the plane $x = 0$. The vertical axis corresponds to the density of the phantom.*

direction. Thus, if more detecting sites (aka. cone vertices) are available, the quality of interpolation/approximation would be better. However, there is a tradeoff between the quality of the reconstruction and the economics of having a more compact detector with a shorter scan time. We believe that the detector geometry shown in 2(a) is one of the most challenging admissible geometries.

For the opening angles ψ, we considered 180 uniformly distributed nodes along $(0, \pi)$. For the central axis directions, a triangular mesh on the unit sphere $\mathbb{S}^2$ with 7446 nodes was generated using the algorithm given in [37]. The discretization of the Laplace-Beltrami operator on $\mathbb{S}^2$ was done by a linear approximation of the gradient and divergence operators on each triangle followed by a weighted averaging over the first ring of each vertex in terms of the triangle area [38].

The Radon projections, for 128 nodes of uniformly sampled $s \in [-1, 1]$ from $Rf(\beta, u \cdot \beta)$ at each direction $\beta \in \mathbb{S}^2$ (with a total of 7446 points), were obtained by using `MATLAB`'s curve fitting toolbox `cftool` with spline fitting. Finally, we used the filtered back-projection algorithm (3) to invert

the Radon transform, and obtained the reconstruction on an array of cubic voxels of size $90 \times 90 \times 90$ which were obtained by uniform discretization of $[-1, 1]^3$.

Figure 3 includes the results of the numerical implementation of the inversion formula (14). Here, part (a) and (b) depict the cross-section of the reconstruction by the plane $x = 0$ and the comparison of z-axis profiles of the phantom and the reconstruction, respectively. The corresponding plots for the reconstruction from cone projections that are contaminated with 5% Gaussian white noise are shown in parts (c) and (d), respectively. The L^2-error values for the reconstructions from Compton data without additive noise and with 5% Gaussian noise were 0.3427 and 0.3779, respectively.

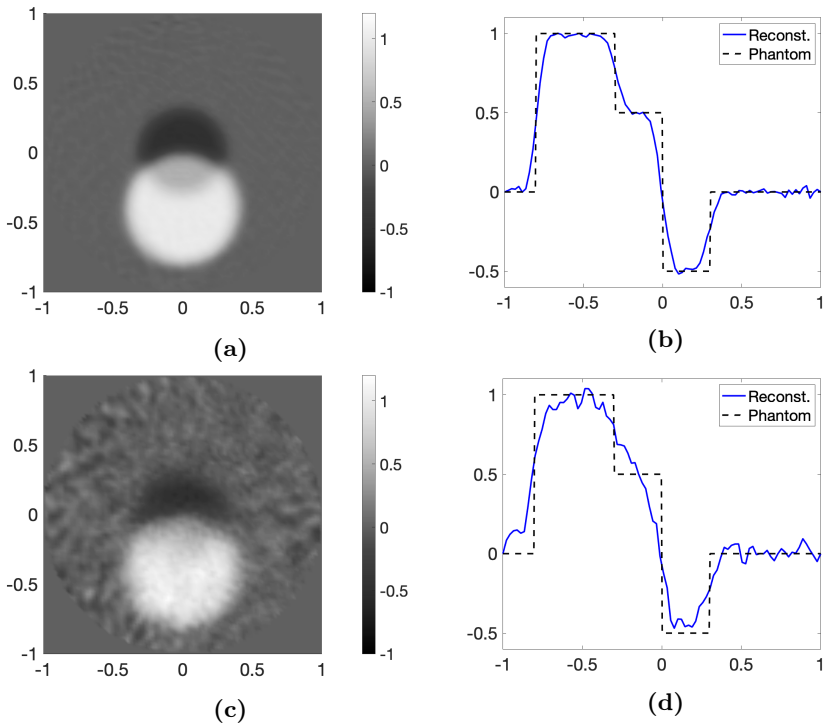

Figure 3. *The reconstruction (of size* $90 \times 90 \times 90$*) of the phantom shown in fig. 2 via* (14) *from its cone projections that are synthetically simulated using 360 vertices* u *(represented by black dots on the sphere in fig. 2(a)), 7446 directions* $\beta \in \mathbb{S}^2$ *and 180 opening angles* ψ*.* **(a)** *The cross-section of the reconstruction by the plane* $x = 0$*.* **(b)** *The comparison of z-axis profiles of the phantom and the reconstruction.* **(c)** *The cross-section by the plane* $x = 0$ *of the reconstruction from cone projections that are contaminated with 5% Gaussian white noise.* **(d)** *The comparison of z-axis profiles of the phantom and the reconstruction from noisy cone projections.*

The results of the numerical implementation of the inversion formula (19) are provided in fig. 4. The cross-section of the reconstruction by the plane

$x = 0$ and the comparison of z-axis profiles of the phantom and the reconstruction are given in fig. 4(a) and fig. 4(b), respectively. Figures 4(c) and 4(d) show the corresponding plots for the reconstruction from cone projections that are contaminated with 5% Gaussian white noise, respectively. The L^2-error values for the reconstructions from Compton data without additive noise and with 5% Gaussian noise were 0.3504 and 0.3554, respectively.

According to figures 3 and 4, the quality of reconstruction obtained by using the formula (19) is worse than the one obtained by using (14). However, the former is more robust to noise. The lower quality of the reconstruction may be explained by the extra step of integration over the unit sphere with a singular kernel present in the formula (19). On the other hand, since this amounts to a weighted average over the spherical variable, it might be the reason for the robustness to noise. An amplification of the error is expected in both formulas because the inversion of the Compton transform, which is a finite order smoothing operator, is a mildly ill-posed problem [12, 14, 15].

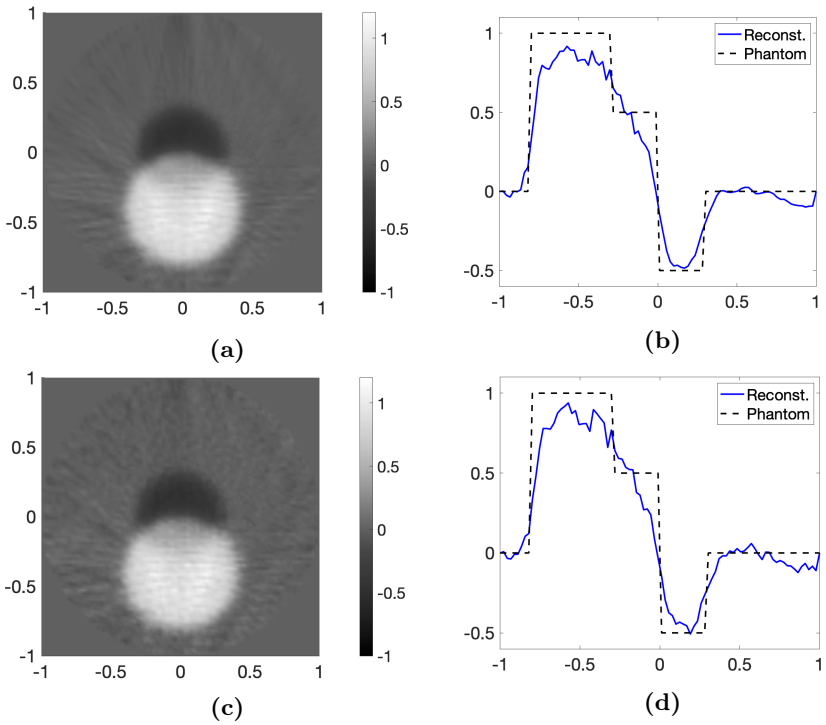

Figure 4. *The reconstruction (of size* $90 \times 90 \times 90$*) via* (19) *of the phantom from the cone projections that are described in fig. 3.* **(a)** *The cross-section of the reconstruction by the plane* $x = 0$*.* **(b)** *The comparison of z-axis profiles of the phantom and the reconstruction.* **(c)** *The cross-section by the plane* $x = 0$ *of the reconstruction from cone projections that are contaminated with 5% Gaussian white noise.* **(d)** *The comparison of z-axis profiles of the phantom and the reconstruction from noisy cone projections.*

For a comparison, we reimplemented the inversion formula previously obtained by using the convolution kernel $h(t) = |t|$ (see [21, eq. (14)]) in the present experimental setting. Although it led to successful reconstructions from a 10% noisy Compton data of size $1080 \times 30054 \times 90$ in the case of a spherical detector geometry [21], it failed to produce a meaningful result when we used a 5% noisy Compton data of size $360 \times 7446 \times 180$ corresponding to the detector geometry shown in fig. 2(a). This can be attributed to the use of a more challenging detector geometry and much coarser forward data this time. We then implemented formulas (19) and [21, eq. (14)] using 10% noisy Compton data of size $1080 \times 30054 \times 90$ obtained from spherical detectors in the case of a ball phantom of radius 0.5 with center at the origin. The results of the reconstructions, depicted in Fig. 5, show that the formula (19) leads to a considerable improvement in stability in comparison to [21, eq. (14)].

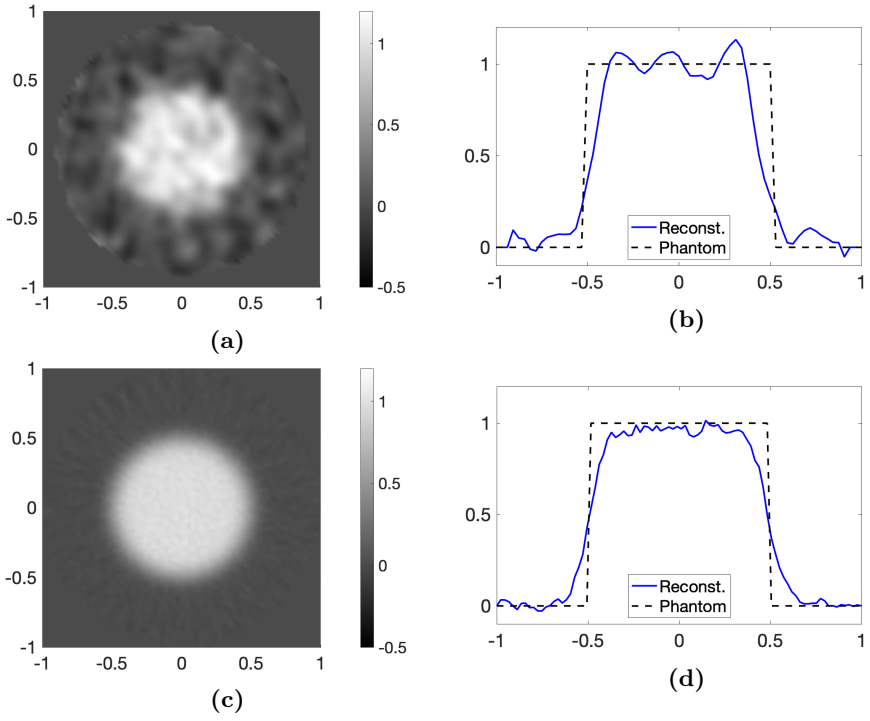

Figure 5. **(a)** *The cross-section (by the plane $x = 0$) and* **(b)** *x-axis profile of the reconstruction (of size $90 \times 90 \times 90$) of a ball phantom of radius 0.5 centered at the origin from 10% noisy Compton data of size $1080 \times 30054 \times 90$ obtained from spherical detectors via [21, eq. (14)].* **(c)** *and* **(d)** *The corresponding plots of the reconstruction via* (19).

6. Conclusions

We proposed new analytical inversion formulas for the n-dimensional cone/ Compton transform in the case of pure surface measure on the cones, which is an idealized solution to the problem of image reconstruction from Compton camera measurements. We proved that weighted averaging of the Compton projections of a source distribution over the opening angles leads to a spherical convolution of the Radon transform of that distribution. This relation enabled us to invert the Compton transform in two steps: first performing spherical deconvolution to obtain the Radon transform, and then applying well-known techniques for Radon transform inversion to recover the original function. Different choices of the convolution kernel led to various methods for the recovery of the Radon projections, hence various inversion formulas for the Compton transform. We developed two analytic inversion formulas for the n-dimensional Compton transform that hold for a variety of Compton detector geometries. The numerical implementations in dimension three demonstrated that the proposed inversion formulas lead to considerable improvement in the quality of reconstruction with significantly coarser data when compared to our previously obtained inversion algorithms.

Appendix

Proof of eq. (6). Let $\sigma, \beta \in \mathbb{S}^{n-1}$. Suppose that A rotates the north pole e_n of $\mathbb{S}^{n-1}$ to σ, that is $\sigma = Ae_n$. Let $A^{-1}\beta =: \eta \in \mathbb{S}^{n-1}$. Since the Lebesgue measure on the sphere is rotation invariant, we have

$$\begin{aligned} w_\beta(\sigma) = Fh_\beta(\sigma) &= \int\limits_{\mathbb{S}^{n-1}} \delta(\omega\cdot\sigma)h(\omega\cdot\beta)d\omega \\ &= \int\limits_{\mathbb{S}^{n-1}} \delta(A\omega\cdot\sigma)h(A\omega\cdot\beta)d\omega = \int\limits_{\mathbb{S}^{n-1}} \delta(\omega_n)h(\omega\cdot\eta)d\omega. \end{aligned}$$

Now, if $n = 2$, then

$$\begin{aligned} &\int\limits_{\mathbb{S}^1} \delta(\omega_2)h(\omega\cdot\eta)d\omega \\ &= \int\limits_{-1}^{1} \delta(\omega_2)\left[h\big(\sqrt{1-\omega_2^2}\eta_1 + \omega_2\eta_2\big) + h\big(-\sqrt{1-\omega_2^2}\eta_1 - \omega_2\eta_2\big)\right]\frac{d\omega_2}{\sqrt{1-\omega_2^2}} \\ &= h(\eta_1) + h(-\eta_1) = h\big(\sqrt{1-\eta_2^2}\big) + h\big(-\sqrt{1-\eta_2^2}\big), \end{aligned}$$

and, if $n \geqslant 3$, then

$$\int_{\mathbb{S}^{n-1}} \delta(\omega_n) h(\omega \cdot \eta) d\omega = \int_{\mathbb{S}^{n-2}} \int_{-1}^{1} \delta(\omega_n) h(\sqrt{1-\omega_n^2}\zeta \cdot \bar{\eta} + \omega_n \eta_n)(1-\omega_n^2)^{\frac{n-3}{2}} d\omega_n d\zeta$$
$$= \int_{\mathbb{S}^{n-2}} h(\zeta \cdot \bar{\eta}) d\zeta,$$

where $\eta = (\bar{\eta}, \eta_n)$. Again since the Lebesgue measure on the sphere $\mathbb{S}^{n-2}$ is rotation invariant, we obtain

$$\int_{\mathbb{S}^{n-2}} h(\zeta \cdot \bar{\eta}) d\zeta = |\mathbb{S}^{n-3}| \int_0^{\pi} h(|\bar{\eta}| \cos\phi)(\sin\phi)^{n-3} d\phi$$
$$= |\mathbb{S}^{n-3}| \int_{-1}^{1} h(|\bar{\eta}| t)(1-t^2)^{\frac{n-4}{2}} dt.$$

Since $\eta_n = \eta \cdot e_n = A^{-1}\beta \cdot A^{-1}\sigma = \beta \cdot \sigma$, we have

$$|\bar{\eta}| = \sqrt{|\eta|^2 - \eta_n^2} = \sqrt{1 - (\beta \cdot \sigma)^2},$$

and thus,

$$w_\beta(\sigma) = w(\sigma \cdot \beta) = \begin{cases} h(\sqrt{1-(\sigma\cdot\beta)^2}) + h(-\sqrt{1-(\sigma\cdot\beta)^2}), & n = 2, \\ |\mathbb{S}^{n-3}| \int_{-1}^{1} h(\sqrt{1-(\sigma\cdot\beta)^2}\, t)(1-t^2)^{\frac{n-4}{2}} dt, & n \geqslant 3, \end{cases}$$

which implies (6). □

Acknowledgements

The author thanks P. Kuchment for numerous discussions. The author is also grateful to the referees for careful reading of the manuscript and for the comments, corrections, and suggestions that led to significant improvements of the paper. This work was supported in part by the National Science Foundation through Award DMS-2206279.

References

[1] M. Allmaras, D. Darrow, Y. Hristova, G. Kanschat, and P. Kuchment, "Detecting small low emission radiating sources," *Inverse Problems and Imaging*, vol. 7, no. 1, pp. 47–79, 2013.

[2] R. Basko, G. L. Zeng, and G. T. Gullberg, "Application of spherical harmonics to image reconstruction for the Compton camera," *Physics in Medicine and Biology*, vol. 43, no. 4, p. 887, 1998.

[3] M. J. Cree and P. J. Bones, "Towards direct reconstruction from a gamma camera based on Compton scattering," *IEEE transactions on medical imaging*, vol. 13, no. 2, pp. 398–407, 1994.

[4] V. Maxim, M. Frandeş, and R. Prost, "Analytical inversion of the Compton transform using the full set of available projections," *Inverse Problems*, vol. 25, no. 9, p. 095001, 2009.
[5] M. K. Nguyen and T. Truong, "On an integral transform and its inverse in nuclear imaging," *Inverse Problems*, vol. 18, no. 1, p. 265, 2002.
[6] W. Rogers, N. Clinthorne, and A. Bolozdynya, "Compton cameras for nuclear medical imaging," in *Emission Tomography: the Fundamentals of PET and SPECT*, pp. 383–419, 2004.
[7] B. Smith, "Reconstruction methods and completeness conditions for two Compton data models," *JOSA A*, vol. 22, no. 3, pp. 445–459, 2005.
[8] F. Terzioglu, P. Kuchment, and L. Kunyansky, "Compton camera imaging and the cone transform: a brief overview," *Inverse Problems*, vol. 34, no. 5, p. 054002, 2018.
[9] E. Muñoz, J. Barrio, J. Bernabéu, A. Etxebeste, C. Lacasta, G. Llosá, A. Ros, J. Roser, and J. F. Oliver, "Study and comparison of different sensitivity models for a two-plane Compton camera," *Physics in Medicine & Biology*, vol. 63, no. 13, p. 135004, 2018.
[10] V. Maxim, "Enhancement of Compton camera images reconstructed by inversion of a conical Radon transform," *Inverse Problems*, vol. 35, no. 1, p. 014001, 2018.
[11] P. Kuchment and F. Terzioglu, "Inversion of weighted divergent beam and cone transforms," *Inverse Problems & Imaging*, vol. 11, no. 6, pp. 1071–1090, 2017.
[12] V. Palamodov, "Reconstruction from cone integral transforms," *Inverse Problems*, vol. 33, no. 10, p. 104001, 2017.
[13] M. Haltmeier, "Exact reconstruction formulas for a Radon transform over cones," *Inverse Problems*, vol. 30, no. 3, p. 035001, 2014.
[14] F. Terzioglu, "Some analytic properties of the cone transform," *Inverse Problems*, vol. 35, p. 034002, 2019.
[15] Y. Zhang, "Recovery of singularities for the weighted cone transform appearing in the Compton camera imaging," *Inverse Problems*, 2019.
[16] G. Ambartsoumian, "Inversion of the V-line Radon transform in a disc and its applications in imaging," *Computers & Mathematics with Applications*, vol. 64, no. 3, pp. 260–265, 2012.
[17] R. Gouia-Zarrad and G. Ambartsoumian, "Exact inversion of the conical Radon transform with a fixed opening angle," *Inverse Problems*, vol. 30, no. 4, p. 045007, 2014.
[18] R. Gouia-Zarrad, "Analytical reconstruction formula for n-dimensional conical Radon transform," *Computers & Mathematics with Applications*, vol. 68, no. 9, pp. 1016–1023, 2014.
[19] M. K. Nguyen, T. T. Truong, and P. Grangeat, "Radon transforms on a class of cones with fixed axis direction," *Journal of Physics A: Mathematical and General*, vol. 38, no. 37, p. 8003, 2005.
[20] F. Terzioglu, "Some inversion formulas for the cone transform," *Inverse Problems*, vol. 31, no. 11, p. 115010, 2015.
[21] P. Kuchment and F. Terzioglu, "Three-dimensional image reconstruction from Compton camera data," *SIAM Journal on Imaging Sciences*, vol. 9, no. 4, pp. 1708–1725, 2016.
[22] K. Kwon, "An inversion of the conical Radon transform arising in the Compton camera with helical movement," *Biomedical engineering letters*, vol. 9, no. 2, pp. 233–243, 2019.
[23] S. Moon and K. Kwon, "Inversion formula for the conical Radon transform arising in a single first semicircle second Compton camera with rotation," *Japan Journal of Industrial and Applied Mathematics*, vol. 36, no. 3, pp. 989–1004, 2019.
[24] C.-Y. Jung and S. Moon, "Inversion formulas for cone transforms arising in application of Compton cameras," *Inverse Problems*, vol. 31, no. 1, p. 015006, 2015.

[25] C.-Y. Jung and S. Moon, "Exact inversion of the cone transform arising in an application of a Compton camera consisting of line detectors," *SIAM Journal on Imaging Sciences*, vol. 9, no. 2, pp. 520–536, 2016.
[26] S. Moon, "Inversion of the conical Radon transform with vertices on a surface of revolution arising in an application of a Compton camera," *Inverse Problems*, vol. 33, no. 6, 2017.
[27] S. Moon and M. Haltmeier, "Analytic inversion of a conical Radon transform arising in application of Compton cameras on the cylinder," *SIAM Journal on imaging sciences*, vol. 10, no. 2, pp. 535–557, 2017.
[28] I. M. Gel'fand, S. G. Gindikin, and M. I. Graev, *Selected Topics in Integral Geometry*, vol. 220. American Mathematical Soc., 2003.
[29] S. Helgason, *Integral Geometry and Radon Transforms*. Springer Science & Business Media, 2010.
[30] F. Natterer, *The Mathematics of Computerized Tomography*, vol. 32. SIAM, 1986.
[31] P. Funk, "Über flächen mit lauter geschlossenen geodätischen linien," *Mathematische Annalen*, vol. 74, no. 2, pp. 278–300, 1913.
[32] B. Rubin, *Introduction to Radon Transforms*, vol. 160. Cambridge University Press, 2015.
[33] P. Kuchment, *The Radon Transform and Medical Imaging*, vol. 85. SIAM, 2014.
[34] R. Chapling, "A hypergeometric integral with applications to the fundamental solution of Laplace's equation on hyperspheres," *SIGMA. Symmetry, Integrability and Geometry: Methods and Applications*, vol. 12, p. 079, 2016.
[35] I. S. Gradshteyn and I. M. Ryzhik, *Table of Integrals, Series, and Products*. Elsevier, 2007.
[36] F. Terzioglu, "Exact inversion of an integral transform arising in Compton camera imaging," *Journal of Medical Imaging*, vol. 7, no. 3, p. 032504, 2020.
[37] P.-O. Persson and G. Strang, "A simple mesh generator in MATLAB," *SIAM review*, vol. 46, no. 2, pp. 329–345, 2004.
[38] G. Xu, "Discrete Laplace–Beltrami operators and their convergence," *Computer aided geometric design*, vol. 21, no. 8, pp. 767–784, 2004.

Department of Mathematics, North Carolina State University, Raleigh, NC 27695

Email address, Corresponding author: `fterzioglu@ncsu.edu`